Pergamon

Int. J. Heat Mass Transfer. Vol. 39, No. 1, pp. 97–108, 1996

0017-9310/96 $9.50+0.00

0017-9310(95)00057-6

Method of heat and mass transfer enhancement in film evaporation

G. S. ZHENG and W. M. WOREK†

University of Illinois at Chicago, Department of Mechanical Engineering (m/c 251), 842 West Taylor Street, Chicago, IL 60607-7022, U.S.A.

(*Received* 8 *November* 1993 *and in final form* 17 *February* 1995)

Abstract—Combined heat and mass transfer processes that occur when water evaporates from a flowing film have been investigated. The major emphasis of this work studied methods to enhance heat and mass transfer rates from the film. A fiber-optic holographic interferometer was used to measure the local heat and mass transfer coefficients from the air–liquid interface, and a set of thermocouples and a dewpoint hygrometer were used to measure the average heat and mass transfer rates in the system. First, without utilizing any enhancement techniques, the local and average transfer rates from the water solution were determined, then a mechanical method for enhancing the heat and mass transfer rates was investigated. In this method, 2 mm glass rods were used to disturb the liquid film flow, which also disturbed the flow of the air stream. The local temperature and concentration distributions were calculated and used to evaluate the local Nusselt and Sherwood numbers. It was observed that average Nusselt number Nu_{av} and average Sherwood number Sh_{av} for the water solution have a maximum which depends on the pitch of the glass rods.

INTRODUCTION

Combined heat and mass transfer from falling liquid films with one solid–liquid and one gas–liquid interface are frequently encountered in engineering processes. Flow in vertical condensers, solar-assisted liquid desiccant absorption air-conditioners, absorption chillers, film reactors, wetted-wall columns and water runways are examples. A well-known method to enhance the heat transfer from a surface is to roughen the surface either randomly with grains of sand, or by use of regular geometric roughness elements on the surface. Surfaces roughened with discrete small square ribs have been widely used in the pursuit of heat transfer enhancement in duct flow. There have been a number of investigations on the heat transfer from the roughened wall of a duct. Most of this work has been experimental and semi-theoretical studies of the mean values of heat transfer from such surfaces. The flow and turbulence distributions over such surfaces have also been studied in some detail. However, relatively little has been done on the distribution of local heat and mass transfer coefficients on roughened surfaces. Also, little work has been done on the determination of the optimum pitch of roughness elements for a given flow rate.

Monolayers have long been known to retard evaporation. Recently, the method of enhancement of the heat and mass transfer from a falling film has received considerable attention in evaporation and sorption systems [1–4]. The objective of this study was to investigate the distribution of local heat and mass transfer coefficients in an evaporation process at the air–liquid interface and to determine the effect of introducing rods to disturb the liquid and air flow field and to enhance the heat and mass transfer rates.

Induced convection in mass transfer processes can increase heat and mass transfer rates several times greater than those estimated from molecular properties. Convection can be produced through buoyancy effects and surface forces generated by the process, or through artificial means, such as stirring or vibration. The influence of monomolecular films and small surface waves on the absorption of carbon dioxide into water has been investigated by Boyd and Marchello [5]. It was found that the effective diffusivity with the occurrence of ripples by agitated rods was much greater than the case when no ripples were observed on the liquid film. Banerjee *et al.* [6] proposed a model for the film absorption process in wave motion, which takes into account eddies formed within the film by the passage of waves. Their predictions of the liquid phase mass transfer coefficients are in agreement with experiments in the published literature. Berger and Hau [7] used an electrochemical analogy technique to determine the heat transfer distribution in pipes roughened with square small ribs. Nelson and Wood [8] proposed a numerical method to model the water evaporation rate in a glazed collector/regenerator which is a component of an open-cycle absorption refrigeration system. Han *et al.* [9] investigated the effect of the agitated rib angle orientation on the local heat transfer distributions and on the pressure drop in a square channel with two opposite in-line ribbed

† Author to whom correspondence should be addressed.

NOMENCLATURE

C_A^*	dimensionless concentration of water vapor
c_p	specific heat at constant pressure [J kg^{-1} K^{-1}]
D	diameter of the rods [m]
D_{AB}	binary mass diffusion coefficient [m^2 s^{-1}]
D_h	hydraulic diameter [m]
h	convection heat transfer coefficient [W m^{-2} K^{-1}]
H_a	total air enthalpy [kW]
H_{evap}	energy lost by the film by due to evaporation [kW]
H_l	total liquid enthalpy [kW]
h_{fg}	heat of vaporization of water [kJ kg^{-1}]
h_m	convection mass transfer coefficient [m s^{-1}]
i_a	air enthalpy [kJ kg^{-1}]
i_l	liquid enthalpy [kJ kg^{-1}]
K_{air}	thermal conductivity of air [W m^{-1} K^{-1}]
L	the rod pitch [m]
$\dot{m}$	mass flow rate [kg s^{-1}]
$\dot{M}$	mass flow rate of water evaporated [kg s^{-1}]
Nu_{av}	average Nusselt number
Nu_l	local Nusselt number
Q_{conv}	convection transfer from the solution surface [kW]
Q_{in}	energy input from the heating plate [kW]
$\dot{q}$	total heat transfer from the liquid to the air stream [kW]
Sh_{av}	average Sherwood number
Sh_l	local Sherwood number
T	temperature [K]
T^*	dimensionless temperature
W	humidity ratio [kg water per kg dry air]
y^*	dimensionless position.

Greek Symbol

ρ	density.

Subscripts

a	air phase
av	average value
h	heating plate
i	inlet
l	liquid phase
o	outlet
s	interface
w	water vapor
x	local condition on a surface.

walls and Sparrow and Tao [10] investigated the heat transfer and pressure drop response to periodic, rod-type disturbance elements situated adjacent to one principal wall and oriented transverse to the flow direction in a flat rectangular duct.

A number of studies of combined heat and mass transfer processes using holographic interferometry have been reported [11–14]. The results obtained from the holograms provide detailed information on the transport processes. The main advantage of this optical method is its non-intrusive nature and the fact that information about the whole field can be obtained by evaluating the interferograms. Evaporation of water into an air stream is a combined heat and mass transfer process. Typically such processes cannot be easily visualized, therefore a laser holographic interferometric method is used in this study to help gain insight, both qualitatively and quantitatively, into the combined heat and mass transfer processes that occur in film evaporation.

The measurement techniques used in this study are a two-wavelength, fiber-optic, holographic interferometer measuring the local heat and mass transfer coefficients and a chilled-mirror hygrometer and a data acquisition system with thermocouples measuring the average heat and mass transfer coefficients. Pyrex glass rods with a diameter of 2 mm are used to agitate the solution as it flows in the system. The effects of the rod pitch number on the heat and mass transfer rates from a flowing film of water are investigated.

EXPERIMENTAL TECHNIQUE AND APPARATUS

The experimental set-up for investigating the heat and mass transfer processes at the air/film interface, in an inclined channel, is shown schematically in Fig. 1. The system consists of a test chamber, a heating system, an air supply system and a liquid solution supply system. The test chamber, shown as Fig. 2, is a rectangular enclosure [20.3 cm (8 in) × 2.54 cm (1 in) × 55.6 cm (21.9 in)] which is supported by a variable angle steel frame. The tray of the steel frame is inclined at an angle of 6.5°. There are four adjustable screws beneath the test cell to level the test chamber. The side walls and the lid of the test chamber are made of 9.5 mm (3/8 in) thick clear lexan plastic and the bottom of the enclosure is made of an 8.0 mm (5/16 in) thick stainless steel plate. Pyrex glass rods having a diameter of 2 mm, as shown in Fig. 3, are mounted on the stainless steel plate normal to the flow direction to agitate the liquid film as it flows down the inclined plate. The rod pitch L is varied for each test.

There are six 1.27 cm (1/2 in) diameter copper tubes attached to the bottom of the stainless steel plate through which hot water is passed to heat the test

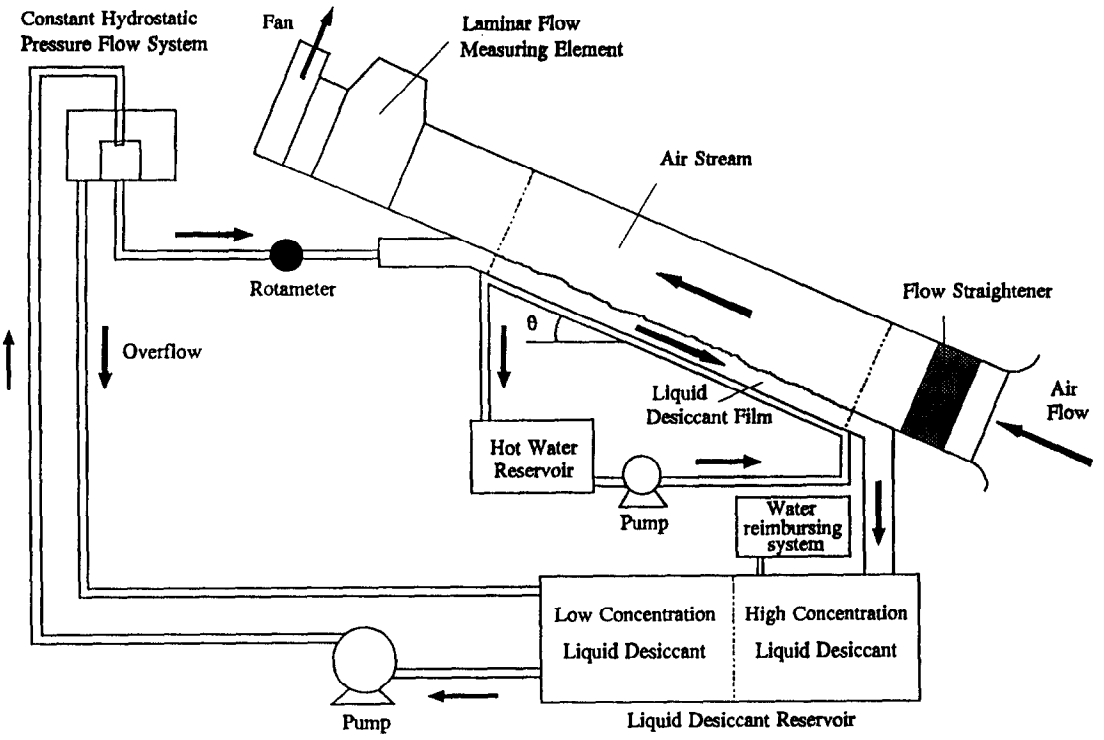

Fig. 1. Schematic diagram of film evaporation test system.

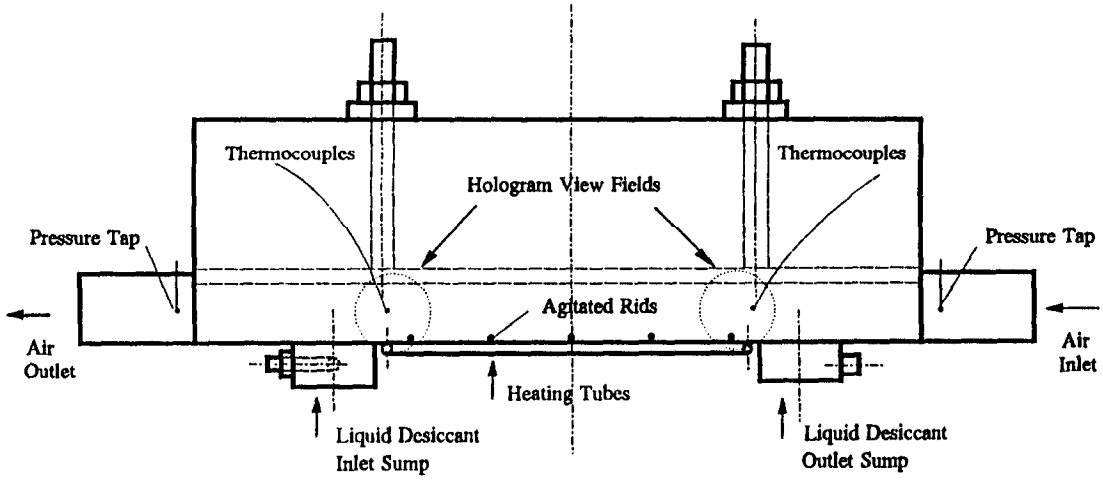

Fig. 2. Schematic of the experimental test chamber.

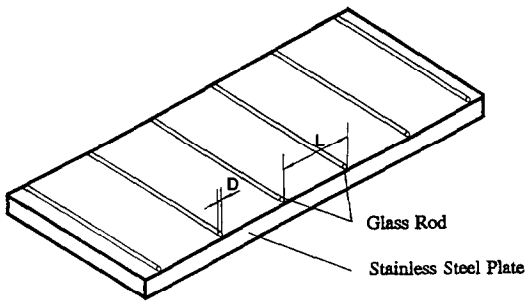

Fig. 3. Schematic of agitated rods on stainless steel plate.

section. The test chamber bottom is insulated to minimize heat losses. There are 39 thermocouples inlaid with a high thermal conductivity epoxy at the bottom of the plate to monitor the variation of the plate temperature. To ensure reliable temperature measurements, all the thermocouples were calibrated in a constant temperature bath. The uncertainty in temperature measurement is $\pm 0.1^{\circ}C$.

A 15.2 cm (6 in) long straight air inlet channel is attached to the test cell to ensure a uniform laminar flow enters the test section. Near the end of the air inlet channel, a small stainless steel tube is inserted

into the air flow to aspirate a sample for the dewpoint measurement and a thermocouple is used to measure the mean inlet temperature. The pressure drop across the channel was measured through small pressure taps in the top of the inlet and outlet channel. The locations of these pressure taps are shown in Fig. 2. The outlet channel is identical to the inlet channel.

The holographic interferometric system and the test section were placed on a 121.9×182.9 cm (4×6 ft) optical table which was supported by high pressure, dry air to avoid vibration. The two lasers used were a 5 mW self-contained air cooled Spectrum Physics He–Ne laser and a 300 mW water-cooled Lexel argon-ion laser. A computer-based data acquisition system was used for data collection. The system was used for monitoring the experiment and for collecting data used to determine the average heat and mass transfer rates.

ANALYTICAL MODEL AND DATA REDUCTION

Performing mass and energy balances on a control element at a distance x from the leading edge of the test system leads to equations that describe the performance of the test section. An energy balance on a differential element of the test channel of length Δx and unit width yields the following equation:

$$H_{l,x} - H_{l,x+\Delta x} + H_{a,x+\Delta x} - H_{a,x} + (Q_{in})_{\Delta x} = 0. \quad (1)$$

The enthalpies carried in and out of the control volume by liquid are given by

$$H_{l,x} = \dot{m}_l i|_x \quad (2)$$

$$H_{l,x+\Delta x} = \dot{m}_l i_l|_{x+\Delta x} \quad (3)$$

and for the air the enthalpies are given by

$$H_{a,x} = \dot{m}_a i_a|_x \quad (4)$$

$$H_{a,x+\Delta x} = \dot{m}_a i_a|_{x+\Delta x}. \quad (5)$$

Due to heat losses in the test system, the thermal energy transfer from the plate to the water solution was found to be 95% of the total heat lost by the heating water which flowed in six copper tubes attached to the bottom of the plate. Therefore, the energy input to the liquid solution from the heating plate is given by

$$Q_{in} = 0.95\dot{m}_h c_{p,w}(T_{h,i} - T_{h,o})\Delta x. \quad (6)$$

An energy balance on the control volume at the air side gives

$$H_{a,x+\Delta x} - H_{a,x} + (Q_{conv} + H_{evap})_{\Delta x} = 0 \quad (7)$$

and energy balance at the liquid film is

$$H_{l,x} - H_{l,x+\Delta x} - (Q_{conv} + H_{evap} - Q_{in})_{\Delta x} = 0. \quad (8)$$

At the interface between the air and the liquid film, energy is transferred from liquid to the air stream from evaporation of the water which depends on the heat of vaporization of water, h_{fg}, and the mass of water evaporated, i.e.

$$H_{evap} = \dot{M}_{\Delta x} h_{fg} = h_{m,x}(\rho_{w,s} - \bar{\rho}_{w,x})\Delta x h_{fg} \quad (9)$$

where $h_{m,x}$ is the local convective mass transfer coefficient.

The energy convected away from the surface of the solution is given by

$$Q_{conv} = h_x(T_s - \bar{T}_{a,x})\Delta x \quad (10)$$

where h_x is the local convective heat transfer coefficient and T_s is the solution surface temperature. The total heat transfer from the liquid to air stream in the control volume is

$$\dot{q}_{\Delta x} = (Q_{conv} + H_{evap})_{\Delta x}. \quad (11)$$

The moisture evaporation rate from the element can be found from the following equation:

$$\dot{M}_{\Delta x} = \dot{m}_{a,x} - \dot{m}_{a,x+\Delta x} = \dot{m}_a(W_x - W_{x+\Delta x}) \quad (12)$$

where W_x is the humidity ratio of the air at the x location.

After substitution of the different terms of equation (7) and (8) from their respective equations, they reduce to the following forms:

$$(\dot{m}_a i_a)_{x+\Delta x} - (\dot{m}_a i_a)_x + h_{m,x}(\rho_{w,s} - \bar{\rho}_{w,x})\Delta x h_{fg} + h_x(T_s - \bar{T}_{a,x})\Delta x = 0 \quad (13)$$

and

$$(\dot{m}_l i_l)_x - (\dot{m}_l i_l)_{x+\Delta x} - h_{m,x}(\rho_{w,s} - \bar{\rho}_{w,x})\Delta x h_{fg} - h_x(T_s - \bar{T}_{a,x})\Delta x + 0.95\dot{m}_h c_{p,w}(T_{h,i} - T_{h,o})\Delta x = 0. \quad (14)$$

In order to solve equations (13) and (14), knowledge of the local heat and mass transfer coefficients and the density and temperature at the interface is required. With the help of the holographic interferometer the local heat and mass transfer coefficients are determined by determining the temperature and density distributions next to the film interface by evaluating the holograms using a two-wavelength interferometer. The principle of a two-wavelength holographic technique to measure temperatures and densities has been described previously by Zheng and Worek [15].

The local Nusselt number at the liquid surface is defined as

$$Nu_l \equiv \frac{h_x D_h}{K_{air}} = \left.\frac{\partial T^*}{\partial y^*}\right|_{y^*=0}. \quad (15)$$

This parameter is equal to the dimensionless temperature gradient at the surface, and it provides a measure of the convection heat transfer occurring at the surface. The average Nusselt number is defined as

$$Nu_{av} = \frac{1}{L}\int_0^L Nu_l \, dx. \quad (16)$$

The local Sherwood number at the liquid surface is defined as

$$Sh_l \equiv \frac{h_{m,x} D_h}{D_{AB}} = \left.\frac{\partial C_A^*}{\partial y^*}\right|_{y^*=0}. \quad (17)$$

This parameter is equal to the dimensionless concentration gradient at the surface and it provides a measure of the convection mass transfer occurring at the surface. The average Sherwood number is defined as

$$Sh_{av} = \frac{1}{L}\int_0^L Sh_l \, dx. \quad (18)$$

ERROR ANALYSIS

The measuring error includes the fringe thickness measurement error, and the temperature and concentration measurement error. The fringe thickness measurement error is inversely proportional to the fringe thickness. In our study, the error was reduced by magnifying the image and using a high-resolution digital imaging processing measurement device. The measurement error is proportional to the resolution of the image processing monitor. In the experiment, the analysis monitor has 512×480 pixels and the measurement error is proportional to half of the vertical length of one monitor pixel divided by the amplification factor and is estimated to be $\pm 2.5\%$.

The error involved in measuring temperature is estimated to be $\pm 0.5\%$ based on standard thermocouple tables. However, the dewpoint temperature measurements are a function of voltage recorded by the data acquisition unit. For d.c. voltage measurements, Hewlett-Packard specifies a maximum error of 0.008% for the range of interest. This corresponds to an error in dewpoint of ± 0.2°C or $\pm 1\%$. Therefore, the relative error involved in measuring concentration in the air stream is estimated to be $\pm 2.5\%$.

The change in the fringe order caused by diffraction error is given by Hauf and Grigull [16]. For the two-wavelength technique, the fringe thickness in the air field is different for each wavelength hologram. Following a procedure similar to that given by Doeblin [17], the errors associated with the measurement of fringes, temperature, concentration, and the measurement error associated with the change in fringe order caused by diffraction error, were combined and estimated. Overall, the total error in the local Nusselt and Sherwood numbers using this procedure was determined to be $\pm 5\%$.

RESULTS

Experiments were conducted for a fixed air and film flow rate and the Reynolds numbers for the air and film were 1350 and 130, respectively. At these operating conditions, a method to agitate mechanically not only the flowing film but also the air stream was used to enhance the heat, and mass transfer from the film was investigated. Glass rods were attached to the plate normal to the flow direction and the spacing of the rods (i.e. rod pitch) varied from 2 to 10 cm for each experiment (i.e. in the results presented a rod pitch of 0 cm was the case of a film having no mechanical disturbance elements added).

All the local temperature and concentration measurements in the air stream in the enclosure were performed using a double-wavelength holographic interferometer. The air stream and liquid film temperature at the inlet and outlet of the test section were measured using thermocouples. The water vapor concentration at the inlet and outlet was measured using an optical dewpoint hygrometer.

Figure 4 shows two holograms which are used to determine the temperature and concentration distributions in the air at the exit of the channel for the case of a pure water film with no disturbances on the plate. Figure 5 shows the two holograms taken in the air at the exit of the channel for a rod pitch L of 5 cm. The shape of the fringes, which represents lines of constant density, illustrates that the air flow is in the laminar flow regime. The fringes at the solution surface are thinner and more condensed which indicates that the temperature and concentration gradients are larger near the solution surface.

The holograms were processed using image processing software and the data were smoothed by the Savinsky–Golay method [18]. With knowledge of the temperature and concentration at the reference point, the temperature and concentration distributions at $x = 0$ in the air field with and without rods were calculated using the two holograms which were con-

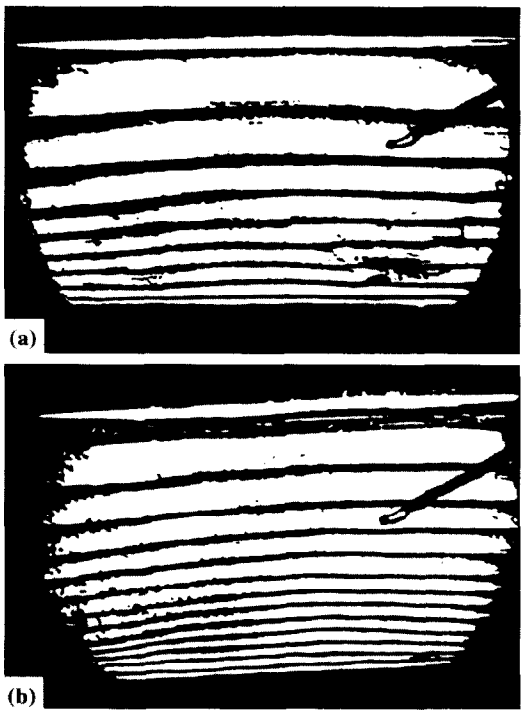

Fig. 4. Holographic interferograms at the air outlet without rods for a pure water solution: (a) constructed by 514.5 nm; (b) constructed by 632.8 nm.

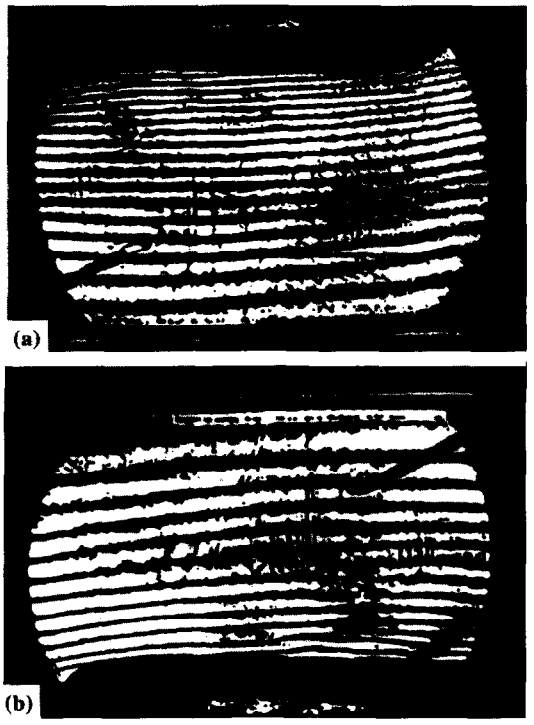

Fig. 5. Holographic interferograms at the air outlet with rod pitch at 5 cm for a pure water solution: (a) constructed by 514.5 nm; (b) constructed by 632.8 nm.

structed at wavelengths of 514.5 and 632.8 nm. The temperature and concentration distributions are shown in Figs. 6 and 7.

For smooth film flow, the local Nusselt and Sherwood numbers are constant along the air–liquid interface in the fully developed region. For an agitated film flow, the flowing film appears like a wave flow and a local maximum heat and mass flux occurs in the front and the tip of each wave, as illustrated in Fig. 8. Moving in the direction of the air flow, the boundary layer begins to develop and the heat and mass transfer coefficients fall gradually until they reach two to three rod diameters upstream of the next rod. The local Nusselt and Sherwood numbers at the interface were calculated for each rod pitch. Figures 9–11 illustrate the variation in the local Nusselt and Sherwood numbers for rod pitches L of 2, 5 and 8 cm. The local Nusselt and Sherwood numbers were integrated to obtain the average Nusselt number and Sherwood number for each pitch number using equations (16) and (18), as shown in Fig. 12.

These results show that the average Nusselt and Sherwood numbers decrease with narrow rod spacing and reach a minimum at a rod pitch L of approximately 2 cm. By adding dye to the flowing film, it was observed that relatively large circulating eddies were generated upstream of the rods and relatively small circulating eddies were generated downstream of the rods. It is believed that with narrow rod spacings, the eddies generated inside the film by the rods interfere with each other, as illustrated in Fig. 13. This results in poor mixing in the liquid film and regions of recirculation in the air stream. This results in low values of Nu_{av} and Sh_{av}.

These results also indicate that the heat and mass transfer from the liquid surface to the air stream is a maximum at a rod pitch L of 5 cm. This shows that by adding rods areas of recirculation are introduced within the film. The hydraulic boundary layer and the thermal boundary layer in the film are disturbed by these eddies. The dominating mechanism of heat and

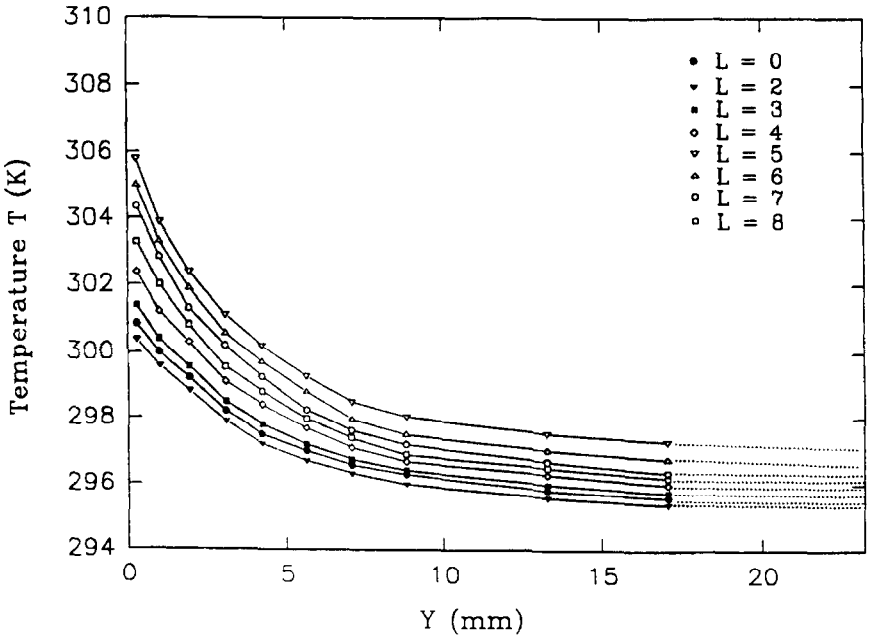

Fig. 6. The temperature distribution at air outlet with different pitch number for pure water solution.

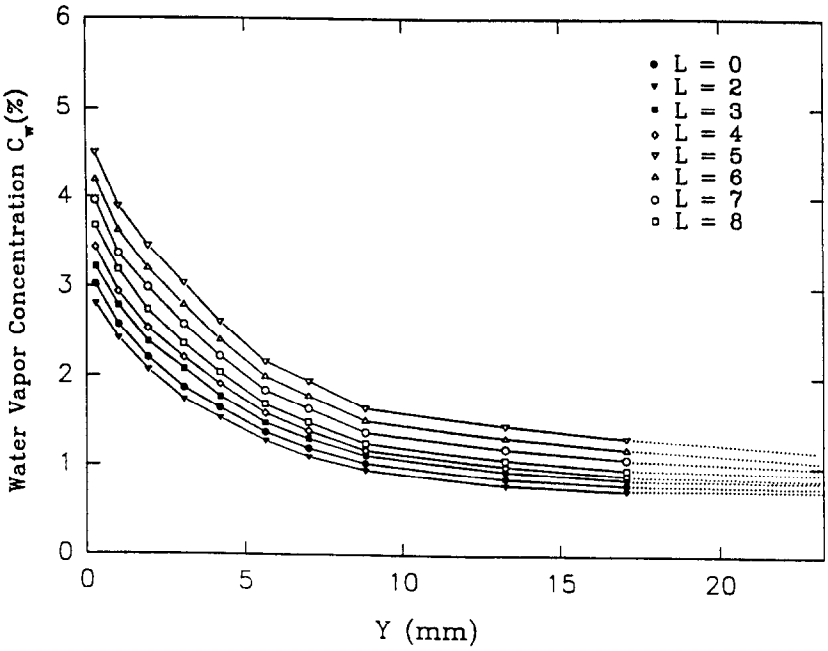

Fig. 7. The concentration distribution at air outlet with different pitch number for pure water solution.

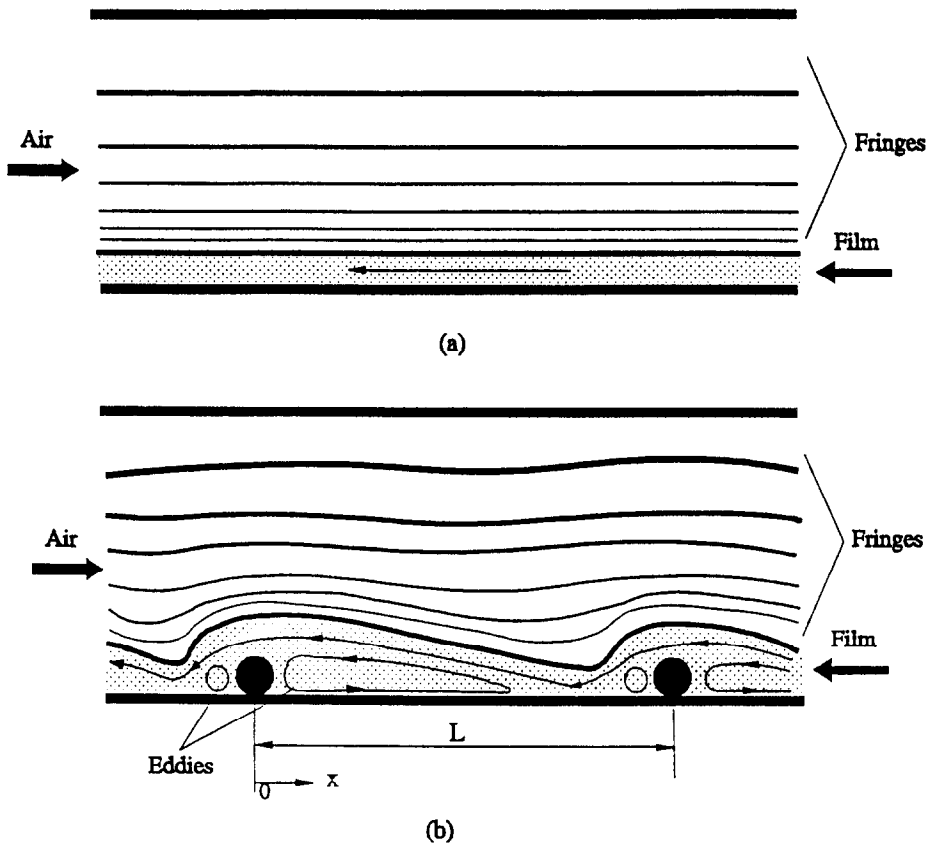

Fig. 8. Schematic of the air and liquid film flow through the channel with fringes forming: (a) no disturbance; (b) with disturbances.

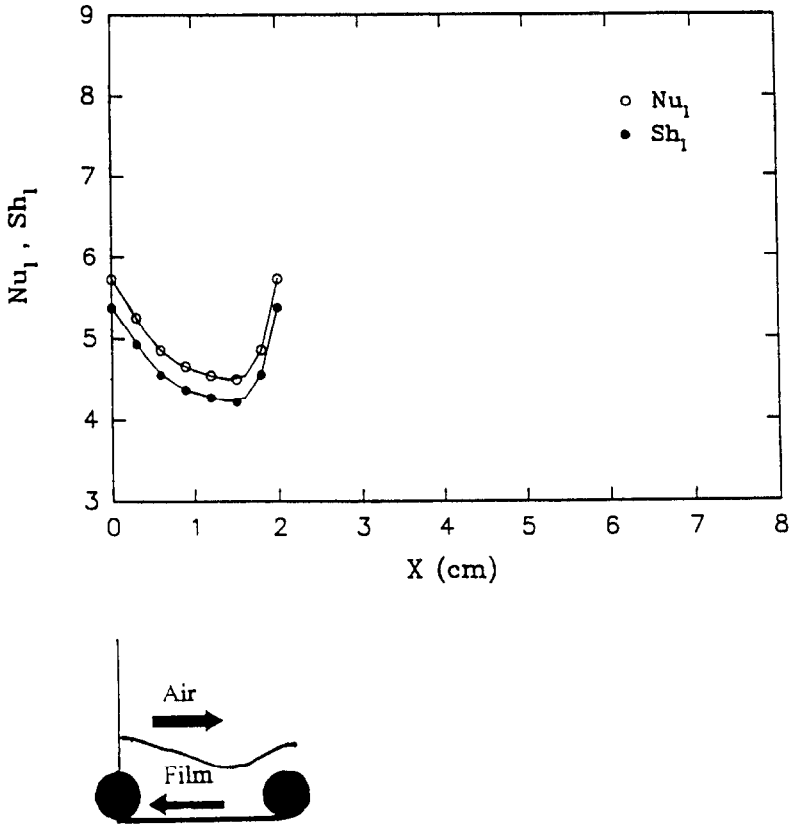

Fig. 9. Local Nusselt and Sherwood number distribution at $L = 2$ cm.

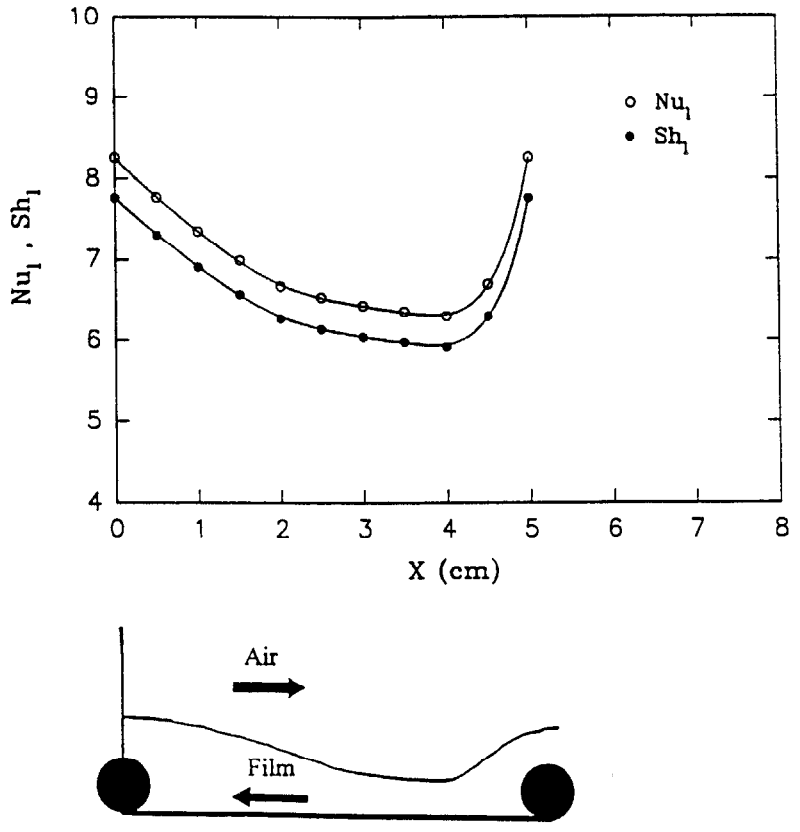

Fig. 10. Local Nusselt and Sherwood number distribution at $L = 5$ cm.

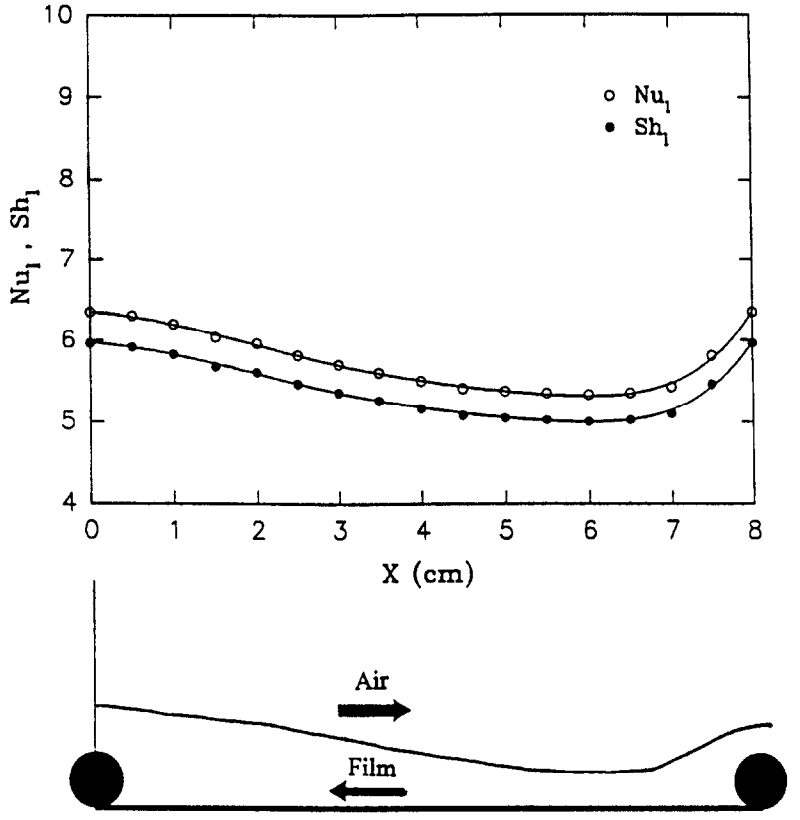

Fig. 11. Local Nusselt and Sherwood number distribution at $L = 8$ cm.

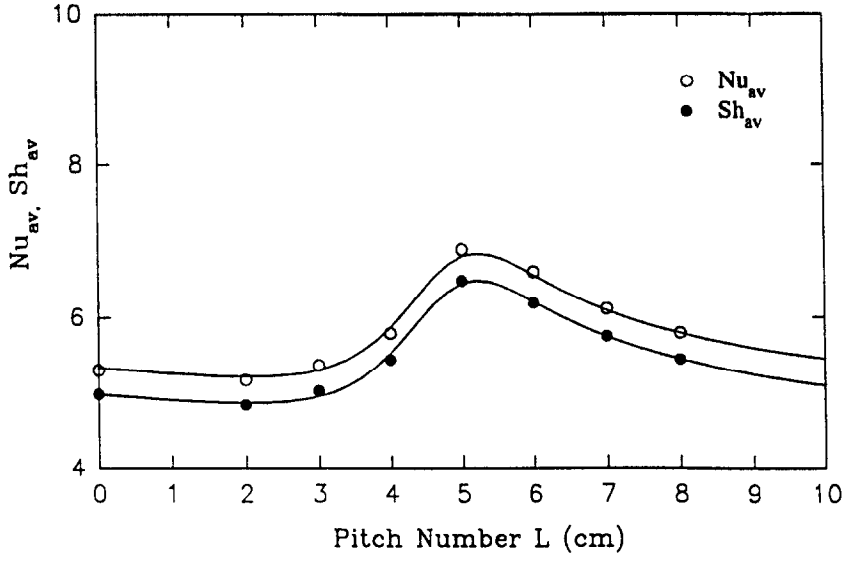

Fig. 12. Average Nusselt and Sherwood number vs agitated rod pitch number with pure water solution.

mass transfer inside the film is by laminar convection which is intermittently mixed by recirculation zones which are associated with the fluid wave structure generated by the rods. In the air stream, the flow separation and reattachment occur due to the presence of the rods and this produces locally very favorable conditions for the heat and mass transfer from the surface of the film. Increasing rod pitch further, the average Nusselt and Sherwood numbers decrease due to the decrease in surface roughness and mixing in the film.

In order to test the evaporation model, attempts were made to reproduce the air stream bulk temperature and concentration at the exit of the channel

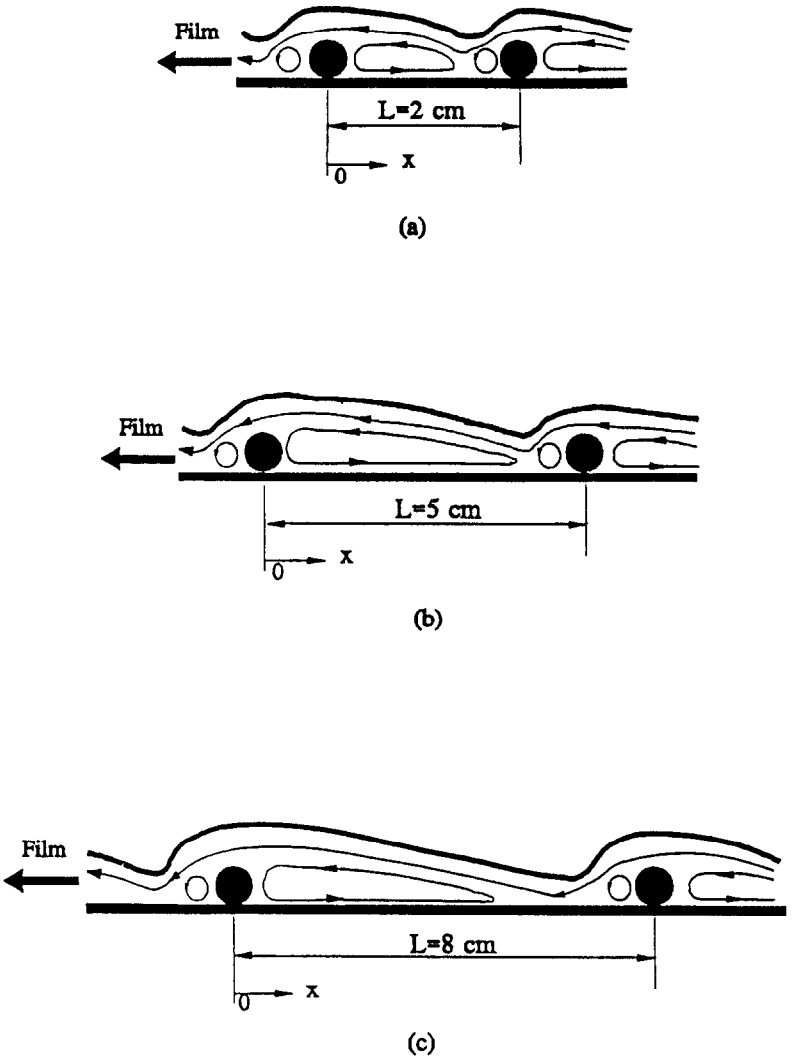

Fig. 13. Schematic diagram of liquid film flow with different rod spacing: (a) $L = 2$ cm; (b) $L = 5$ cm; (c) $L = 8$ cm.

from the inputs of the experimental data by using local heat and mass transfer coefficients calculated from the hologram. The air stream bulk temperature and concentration distribution along the channel are calculated using equations (13) and (14) which are solved using an explicit finite-difference method. The results are shown in Figs. 14 and 15. As one would expect, the model predicts very well the experimental data taken in this research. The predicted exit water vapor concentration shows good agreement with measured values. However, it appears that the model tends to overpredict actual exit air temperature. This discrepancy may be attributed to the fact that the heat lost through the lid and the side walls of the channel is not accounted for in the model. Single instantaneous measurements of the exit air stream conditions may not accurately represent their true values. The measured data also show fluctuations of the exit air temperature and dewpoint during the period of the tests. In spite of all these differences, the closest agreement between the predicted and experimental data is obtained in the prediction of air exit concentration, which is considered to be the most important parameter in the performance evaluation of a method to enhance the combined heat and mass transfer processes in film evaporation.

CONCLUSIONS

In this study, it has been shown that the double-wavelength, fiber-optic, interferometer system is a useful and convenient tool for investigating local and mean heat and mass transfer values on rough surfaces. Local temperature and concentration distributions at the air–liquid interface are obtained with a holographic interferometer and are used to determine the local Nusselt and Sherwood numbers at the air–liquid interface. The results found in this method were compared with the results measured from the thermo-

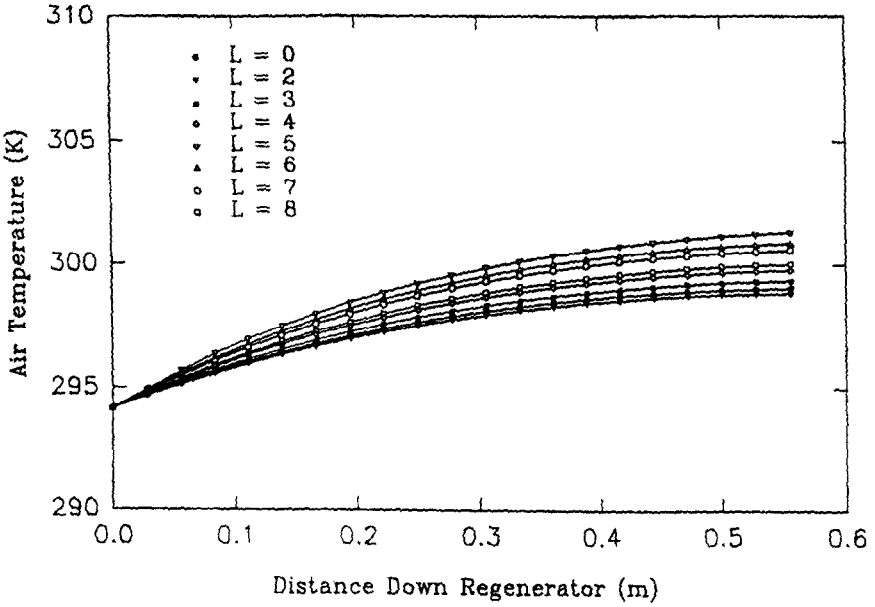

Fig. 14. Variation of the air temperature along the air flow direction in the channel.

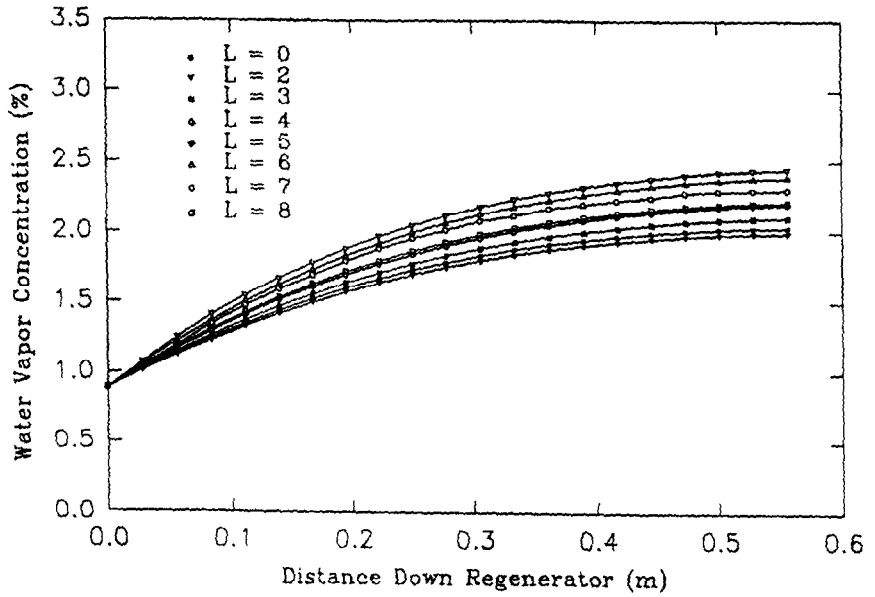

Fig. 15. Variation of the water vapor concentration along the airflow direction in the channel.

couples and a dewpoint hygrometer and are found to be within the experimental error range.

Also, it was found that the combined heat and mass transfer in film evaporation can be enhanced by adding rods to the plate surface to agitate mechanically the flowing film and air stream. By adding the rods in the flowing film, the dominating mechanism of heat and mass transfer inside the film is laminar convection, which is intermittently mixed by circulating zones generated by the rods. The circulating eddies help to enhance the heat and mass transfer inside the film. For agitated film flow, the flowing film appears to be like a wave flow and the maximum location for the heat and mass transfer from the film occurs in the front and the tip of each wave. For the conditions of this experiment, it is found that the optimum rod pitch, which maximizes the heat and mass transfer rates, is 5 cm.

REFERENCES

1. J. C. Han, L. R. Glicksman and W. M. Rohsenow, An investigation of heat transfer and friction for rib-roughened surfaces, *Int. J. Heat Mass Transfer* **21**, 1143–1156 (1978).
2. H. Kozlu, B. B. Mikic and A. T. Patera, Minimum-dissipation heat removal by scale-matched flow desta-

bilization, *Int. J. Heat Mass Transfer* **31,** 2023–2032 (1988).
3. D. A. Dawson and O. Trass, Mass transfer at rough surfaces, *Int. J. Heat Mass Transfer* **15,** 1317–1336 (1972).
4. H. Kozlu, B. B. Mikic and A. T. Patera, Turbulent heat transfer augmentation using microscale disturbances inside the viscous sublayer, *ASME J. Heat Transfer* **114,** 348–353 (1992).
5. D. P. Boyd and J. M. Marchello, Role of films and waves on gas absorption, *Chem. Engng Sci.* **21,** 769–776 (1966).
6. S. Banerjee, E. Rhodes and D. S. Scott, Mass transfer to falling wavy liquid films at low Reynolds numbers. *Chem. Engng Sci.* **22,** 43–48 (1967).
7. F. P. Berger and K.-F., F.-L. Hau, Local mass/heat transfer distribution on surfaces roughened with small square ribs, *Int. J. Heat Mass Transfer* **22,** 1645–1656 (1979).
8. D. J. Nelson and B. D. Wood, Evaporation rate model for a natural convection glazed collector/regenerator, *ASME J. Solar Energy Engng* **112,** 51–57 (1990).
9. J. C. Han, Y. M. Zhang and C. P. Lee, Augmented heat transfer in square channels with parallel, crossed, and V-shaped angled ribs, *ASME J. Heat Transfer* **113,** 590–596 (1991).
10. E. M. Sparrow and W. Q. Tao, Enhanced heat transfer in a flat rectangular duct with streamwise-periodic disturbances at one principal wall, *ASME J. Heat Transfer* **105,** 851–861 (1983).
11. Y. Kurosaki, Experimental study on heat transfer from parallel louvered fin by laser holographic interferometry, *Int. J. Exp. Heat Transfer, Thermodynamics Fluid Mech.* **1,** 59–68 (1988).
12. K. Hijikata and J. Mimatsu, Holographic visualization of pressure distribution on the plate by jet impingement, *Proceedings of the International Symposium on Fluid Control and Measurement*, Vol. 2, pp. 685–695. Tokyo (1985).
13. F. Mayinger and W. Panknin, Holography in Heat and Mass Transfer, *Proceeding of the Fifth International Heat Transfer Conference*, Vol. 6, pp. 28–37 (1974).
14. L. T. Clark, D. C. Koepp and J. J. Thykkuttathil, A three dimensional density field measurement of transonic flow from a square nozzle using holographic interferometry, *J. Fluids Engng* **99,** 737–744 (1977).
15. G. Zheng and W. M. Worek, A holographic method to study combined heat and mass transfer in film sorption. *Int. Commun. Heat Mass Transfer* **19,** 531–540 (1992).
16. W. Hauf and U. Grigull, Optical methods in heat transfer, *Adv. Heat Transfer* **6,** 133–367 (1970).
17. E. O. Doeblin, *Measurement Systems—Application and Design* (4th Edn). McGraw-Hill, New York (1990).
18. R. Annino and R. Driver, *Scientific and Engineering Applications with Personal Computers*. John Wiley, New York (1986).